Exploration on the combustion chemistry of p-xylene: A comprehensive study over wide conditions and comparison among C8H10 isomers

Yuwen Deng, Wenhao Yuan, Sandro Gaïl, Wei Li, Long Zhao, Jiuzhong Yang, Fei Qi, Yuyang Li, Philippe Dagaut

Exploration on the combustion chemistry of *p*-xylene: A comprehensive study over wide conditions and comparison among C_8H_{10} isomers

Yuwen Deng[a,1], Wenhao Yuan[a,1], Sandro Gaïl[c], Wei Li[a], Long Zhao[b], Jiuzhong Yang[b], Fei Qi[a], Yuyang Li[a,*], Philippe Dagaut[c,*]

[a] *School of Mechanical Engineering, Shanghai Jiao Tong University, Shanghai 200240, P. R. China*

[b] *National Synchrotron Radiation Laboratory, University of Science and Technology of China, Hefei, Anhui 230029, P. R. China*

[c] *C.N.R.S.-I.N.S.I.S., Institut de Combustion, Aérothermique, Réactivité et Environnement, 1C, Avenue de la Recherche Scientifique, 45071 Orléans Cedex 2, France*

Abstract: Pyrolysis and oxidation of *p*-xylene over wide conditions were studied in this work in order to provide a comprehensive insight into the combustion chemistry of *p*-xylene. Concerning this goal, the pyrolysis of *p*-xylene was investigated in a flow reactor at pressures from 0.04 to 1 atm over the temperature range of 1000-1600 K. Key radicals, isomers and PAH products including three xylyl isomers, benzyl, xylylene isomers, styrene, benzene, fulvene, indene, naphthalene and phenanthrene, were identified and quantified using synchrotron vacuum ultraviolet photoionization mass spectrometry. The oxidation of *p*-xylene was studied in a jet-stirred reactor at 10 atm, 800-1300 K and equivalence ratios of 0.5-2.0 with a residence time of 0.5 s. Oxidation products were quantified by using gas chromatography combined with mass spectrometry and Fourier transform infrared spectrometry. A kinetic model for *p*-xylene combustion over wide conditions was developed based on our previously proposed *p*-xylene oxidation model and validated against the new experimental measurements in this work and literature reported experimental data, including flow reactor oxidation,

* Corresponding authors. E-mails: yuygli@sjtu.edu.cn (YL), dagaut@cnrs-orleans.fr (PD).
[1] The authors contributed equally to this work.

laminar premixed flame, ignition delay time and laminar burning velocity. In the flow reactor pyrolysis, *p*-xylene mainly undergoes unimolecular decomposition to yield *p*-xylyl, which mainly suffers the H-loss reaction to form *p*-xylylene and isomerization reaction to form *o*-xylyl. The resonantly stabilized fulvenallenyl and benzyl radicals play an important role in the formation of bicyclic and tricyclic PAHs including indene, naphthalene, and phenanthrene. In the JSR oxidation, *p*-xylene is predominantly consumed via H-abstraction by oxygenated radicals such as OH, O, and HO_2 forming *p*-xylyl, which can be oxidized by HO_2 and eventually converted to *p*-methylbenzaldehyde. As the most abundantly produced oxygenated aromatics, further consumption of *p*-methylbenzaldehyde results in the formation of other observed oxygenated aromatics such as cresol, benzofuran, and benzaldehyde. The combustion chemistry of three C_8H_{10} isomers, i.e., *p*-xylene, *o*-xylene, and ethylbenzene, were also compared in terms of pyrolysis and oxidation fuel reactivity, and PAHs formation and growth, showing remarkable fuel isomeric effects.

Keywords: *p*-xylene; flow reactor pyrolysis; jet-stirred reactor oxidation; kinetic model; PAH formation; fuel isomeric effects

Novelty and significance statement

p-Xylene has gained significant attention due to its crucial role in the combustion process of practical fuels. Through comprehensive experimental investigations in a flow reactor (0.04 to 1 atm) and jet-stirred reactor (10 atm, equivalence ratios of 0.5-2.0), as well as dedicated model development and validation, this study provides novel insights into the pyrolysis and oxidation chemistry of *p*-xylene and the formation and growth mechanism of PAHs. Furthermore, a comparison of fuel reactivity and PAHs formation among the combustion of *p*-xylene, *o*-xylene, and ethylbenzene was performed to reveal the fuel isomeric effects on the combustion chemistry of these C_8H_{10} isomers.

Author contributions

Yuwen Deng: Performed research, analyzed data, wrote draft manuscript. **Wenhao Yuan**: Performed research, analyzed data, wrote draft manuscript. **Sandro Gaïl**: Performed research, analyzed data. **Wei Li**: Analyzed data, revised manuscript. **Long Zhao**: Performed research. **Jiuzhong Yang**: Methodology. **Fei Qi**: Methodology. **Yuyang Li**: Designed research, performed research, analyzed data, revised manuscript. **Philippe Dagaut**: Designed research, performed research, analyzed data, revised manuscript.

1. Introduction

Multi-substituted aromatic hydrocarbons like xylenes are common components in commercial gasoline, diesel oils, and jet fuels [1, 2] and are also widely used as surrogate components of these fuels [3-6]. Xylenes are often used as additives to improve the anti-knock propensities of gasoline due to their relatively high octane numbers. Nevertheless, an increased content of xylenes and other aromatic components can increase the formation of polycyclic aromatic hydrocarbons (PAHs) and soot which are known to be carcinogenic and mutagenic. Therefore, experimental and kinetic modeling investigations on xylene combustion are essential for advancing our knowledge of the combustion chemistry of multi-substituted aromatic hydrocarbons and providing insight into the formation mechanisms of PAHs and soot particles. Among the three xylene isomers, *p*-xylene is the most commonly used representative for multi-alkyl substituted aromatics in surrogate gasoline or jet fuels. Besides, previous studies [7-9] have demonstrated that *p*-xylene exhibits different low- to intermediate-temperature oxidation characteristics from *o*-xylene and has different initial decomposition pathways with *o*-xylene and *m*-xylene.

Available experimental studies on the combustion chemistry of *p*-xylene include speciation measurements, reaction parameter measurements, and global combustion characteristic measurements.

Among the speciation measurements, Emdee et al. [10] investigated the oxidation of *p*-xylene in a flow reactor at the pressure of 1 atm, the temperature range of 1093-1199 K and equivalence ratios (ϕ) from 0.47 to 1.7. Oxidation products were measured using gas chromatography combined with mass spectrometry (GC-MS). Their results showed that *p*-xylene was subjected to sequential oxidation of the sidechains on the benzenoid ring and ultimately can be converted to *p*-phthalaldehyde. A detailed kinetic model was also proposed to describe the oxidation pathways of *p*-xylene and its radicals. Lately, Gaïl and Dagaut [11] investigated the oxidation of *p*-xylene in a jet-stirred reactor (JSR) at 1 atm, the temperature range of 900-1300 K, and equivalence ratios from 0.5 to 1.0. Major oxidation products including simple aromatics were measured using GC-MS and a more detailed kinetic model including 160 species and 1175 reactions was developed to interpret experimental observations. Synchrotron vacuum ultraviolet photoionization mass spectrometry (SVUV-PIMS) was used to identify intermediates and products formed in the flame. As an extending work, Yuan et al. [12] studied the laminar premixed flames of *p*-xylene at 0.04 atm with equivalence ratios of 0.75, 1.0, and 1.79 by using SVUV-PIMS. A detailed kinetic model including 397 species and 2697 reactions was also developed to simulate the experimental data. Two reaction parameter measurements were also carried out in previous studies and provide valuable rate coefficients for kinetic model development. Specifically, Hippler et al. [13] studied the thermal decomposition of *p*-xylene in a shock tube at temperatures from 1000 to 1800 K. The rate coefficient for the reaction *p*-xylene $\rightarrow$ *p*-xylyl + H was measured with the aid of UV absorption spectroscopy. Fernandes et al. [14] investigated the thermal decomposition of xylyl radicals in a shock tube by using H-atom resonance absorption spectroscopy (H-ARAS). The overall decomposition rate coefficients of xylyl radicals were measured. Concerning the global combustion characteristic measurements, Battin-Leclerc et al. [7] measured the ignition delay times of *p*-xylene in a shock tube at pressures of 6.7-9 atm, temperatures of 1330-1800 K, and

equivalence ratios of 0.5-2. Shen et al. [15] measured the ignition delay times of *p*-xylene at pressures of 9-45 atm, temperatures of 941-1408 K, and equivalence ratios of 0.5 and 1.0. Natelson et al. [8] investigated the pre-ignition and auto-ignition characteristics of xylene isomers in a flow reactor at 8 atm, 600-850 K, and equivalence ratios of 0.23-0.30. Ji et al. [16] determined laminar burning velocities and extinction strain rates of *p*-xylene at atmospheric pressure and initial temperature of 353 K. As can be concluded from the literature review, available speciation measurements on the combustion chemistry of *p*-xylene are almost exclusively limited to oxidation conditions at 1 atm and flame conditions at low pressure, while the pyrolysis chemistry of *p*-xylene was explored with limited species detected. Table 1 summarizes the experiments related to the speciation and global combustion characteristic measurements of *p*-xylene, which will be utilized to validate the kinetic model developed in this study.

Table 1. Experimental studies of *p*-xylene used for model validation in this work.

Experimental type	*T*/K	*p*/atm	ϕ	References
Jet-stirred reactor oxidation	900-1400	1	0.5, 1.0, 1.5	[11]
	600-1100	1.07	0.5, 1.0, 2.0	[17]
	800-1300	10	0.5, 1.0, 2.0	This work
Flow reactor pyrolysis	1000-1600	0.04-1	∞	This work
Flow reactor oxidation	1155	1	0.86	[10]
Laminar premixed flame	400-2100	0.04	0.75, 1.0, 1.79	[12]
Ignition delay time	1330-1800	6.7-9	0.5, 1.0, 2.0	[7]
	941-1408	10, 40	0.5, 1.0	[15]
Laminar burning velocity	353	1	0.7-1.5	[16, 18]

Regarding the kinetic modeling study, the kinetic models developed by Emdee et al. [10], Gaïl et al. [11], Battin-Leclerc et al. [7], Kukkadapu et al. [19], and Yuan et al. [12] were proposed by validating against limited experimental data, which limits the comprehensive understanding on the combustion chemistry of *p*-xylene. Furthermore, detailed PAH formation and growth mechanism was not included in most of the available kinetic models. The kinetic models proposed for *p*-xylene combustion are summarized in Table 2.

Table 2. Kinetic models of *p*-xylene and their applicability.

Model	*T*/K	*p*/atm	Validation data	Number of species and reactions	References
Emdee et al.	1093-1199	1	flow reactor oxidation	/, /	[10]
Gaïl et al.	900-1300	1	JSR oxidation	160, 1175	[11]
Battin-Leclerc et al.	1330-1800	6.7-9	ignition delay time, flow reactor oxidation	/, 870	[7]
Kukkadapu et al.	900-1500	1, 15, 40	ignition delay time, flow reactor oxidation	/, /	[19]
Yuan et al.	500-2300	0.04	laminar premixed flame	463, 2709	[12]

The main objective of the work is to explore the comprehensive combustion chemistry of *p*-xylene by combining experimental and kinetic modeling methods. First, pyrolysis of *p*-xylene was investigated in a flow reactor at pressures of 0.04-1 atm with the intermediates and products detected by SVUV-PIMS. Oxidation of *p*-xylene was performed in a JSR at the pressure of 10 atm and equivalence ratios of 0.5-2.0 with products detected by GC-MS and GC-TCD and FID (thermal conductivity detector, flame ionisation detector). These measurements provide a major extension to the kinetic database for *p*-xylene. Second, a detailed kinetic model for *p*-xylene combustion was developed and validated against the experimental data measured in this work and literature. Modeling analyses including rate of production (ROP) analysis and sensitivity analysis based on the *p*-xylene model developed in this work were performed to provide insight into the pyrolysis and oxidation chemistry of *p*-xylene, as well as the formation and growth mechanism of PAHs. Finally, the pyrolysis and oxidation fuel reactivity and PAHs formation for *p*-xylene, *o*-xylene, and ethylbenzene were compared to explore the fuel isomeric effects on the combustion chemistry of these C_8H_{10} isomers.

2. Experimental methods

2.1 Flow reactor pyrolysis

The flow reactor pyrolysis experiment was carried out at National Synchrotron Radiation Laboratory in Hefei, China. A detailed introduction about the beamline and the flow reactor apparatus has been reported in our previous work [20, 21]. *p*-Xylene with a purity of >99.5% was purchased

from Aladdin Industrial Inc., Shanghai, China. The experimental conditions of *p*-xylene pyrolysis are outlined in Table 3. After gasification in a vaporizer with a temperature about 20 K higher than the fuel boiling point, *p*-xylene (1 mol%) was blended with the carrier gas argon (99 mol%). A total flow rate of 1000 standard cubic centimeters per minute (sccm) was selected when the above mixture was fed into the flow tube with a 220.0 mm length and 7.0 mm diameter. The flow tube was made of α-alumina to reduce wall catalytic effects [22], A small inner diameter (7.0 mm) was used to ensure strong radial diffusion effects and achieve adequately homogeneous reaction circumstances [23, 24]. In this work, the pressures were maintained at 0.04, 0.2, and 1 atm. Temperature distributions along the centerline of the flow tube were measured by an S-type thermocouple and were used as input parameters in the simulations. Methodologies for intermediate identification and mole fraction evaluation were also reported in detail previously [25]. The uncertainties of the evaluated mole fractions were estimated to be within ±25% for pyrolysis products with measured photoionization cross sections (PICSs) and a factor of 2 for those with estimated PICSs.

Table 3. Experimental conditions of the flow reactor pyrolysis of *p*-xylene.

T/ K	*p*/ atm	Fuel/ mol%	Ar/ mol%	τ/ s
1110-1562	0.04	1.0	99.0	0.018
1152-1493	0.20	1.0	99.0	0.092
1047-1336	1.00	1.0	99.0	0.465

2.2 Jet-stirred reactor oxidation

The JSR oxidation of *p*-xylene was performed at C.N.R.S in Orléans, France with the detailed experimental conditions summarized in Table 4. The experimental apparatus has been introduced in our previous work [26]. Thus, only a brief description is given herein. The JSR is made up of a 40 mm diameter silica sphere from which four nozzles extended inward. A heating wire of ca. 1.5 kW and the highly diluted mixture (0.1 mol% fuel) were utilized to ensure a uniform temperature distribution within the sphere. The delivery of fuel mixture to an atomizer-vaporizer relied on a high-pressure

liquid chromatography pump (Hewlett Packard 1100). Upon analyses, the reactants, products, and stable intermediates were identified after sampling by a fused silica sonic probe. Gas chromatographs equipped with capillary columns (Poraplot-U, Molecular Sieve-5A, DB-5ms, DB-624, Plot Al_2O_3/KCl, Carboplot-P7), TCD, and FID, were used for measuring stable chemical compounds. Their identification was done via analyses of the samples by GC/MS. Ion-trap detectors operating in electron impact positive ionization mode (GC/MS Varian 3800- Saturn 2000) were used. Formaldehyde and carbon dioxide were quantified by GC-FID after hydrogenation on a methaniser (Ni/H_2 catalyst) at the exit of a Poraplot-U GC column. Good repeatability of the mole fractions measurements and a rather good C-balance (100 ± 10%) were observed in the present experiments. The uncertainties of the species mole fractions are estimated to be about ±15% [27]. The experimental data of both flow reactor pyrolysis and JSR oxidation can be found in the *Supplementary Materials*.

Table 4. JSR oxidation experimental conditions.

ϕ	T/ K	p/ atm	Fuel/ mol%	O_2/ mol%	N_2/ mol%	τ/ s
0.50	850-1150	10	0.1	2.100	97.800	0.5
1.00	900-1200	10	0.1	1.050	98.850	0.5
2.00	955-1255	10	0.1	0.525	99.375	0.5

3. Kinetic model

A *p*-xylene (*p*-C_8H_{10}) combustion model consisting of 480 species and 2843 reactions was developed from our previously proposed high-temperature oxidation mechanism of *p*-xylene [12], which includes 397 species and 2697 reversible reactions and was validated against the laminar premixed flame experiments at 0.04 atm and equivalence ratios from 0.75 to 1.79 as listed in Table 5. In this work, the kinetic model was further extended with the initial decomposition reactions of *p*-xylene, the unimolecular decomposition and isomerization reactions of *p*-xylyl, the recombination reactions involving *p*-xylyl and other radicals, as well as the low-to-intermediate temperature oxidation reactions of *p*-xylyl. The pressure-dependent effects of rate coefficients were specially considered in

this work, aiming to accurately capture the decomposition kinetics of *p*-xylene under different pressure conditions. Moreover, the present *p*-xylene model has incorporated the submechanism of PAHs formation derived from our extensively validated toluene model [26] and several literature studies [28-33].

Table 5. Kinetic models used for the development of the *p*-xylene model in this work.

Model object	*T*/K	*p*/atm	Validation data	Number of species and reactions	References
p-xylene	500-2300	0.04	laminar premixed flame	463, 2709	[12]
toluene	800-1730	0.01-10	jet-stirred reactor oxidation, flow reactor pyrolysis, premixed laminar flames, ignition delay times, laminar flame speeds	272, 1698	[26]

The decomposition of *p*-xylene proceeds with the C-H bond dissociation reactions producing *p*-xylyl (*p*-C_8H_9) (R1) or *p*-dimethylphenyl (*p*-$CH_3C_6H_3CH_3$) (R2), or undergoes the C-C bond dissociation reaction producing methylphenyl ($C_6H_4CH_3$) and CH_3 (R3). In addition, H-abstraction reactions by radicals such as H (R4-R5), OH (R6-R7), O (R8-R9), and HO_2 (R10-R11) on the benzylic or phenylic sites of *p*-xylene can also contribute to the initial fuel decomposition. Other routes to *p*-xylene decomposition are the *ipso*-substitution reactions initiated by H and OH, leading to toluene ($A1CH_3$) (R12) and dimethylphenol ($HOCH_3C_6H_3CH_3$) (R13), respectively.

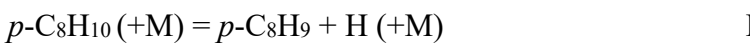

p-C_8H_{10} (+M) = *p*-C_8H_9 + H (+M) R1

p-C_8H_{10} (+M) = *p*-$CH_3C_6H_3CH_3$ + H (+M) R2

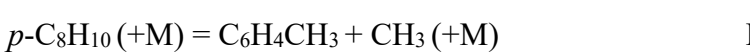

p-C_8H_{10} (+M) = $C_6H_4CH_3$ + CH_3 (+M) R3

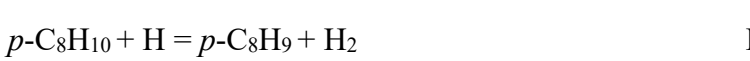

p-C_8H_{10} + H = *p*-C_8H_9 + H_2 R4

p-C_8H_{10} + H = *p*-$CH_3C_6H_3CH_3$ + H_2 R5

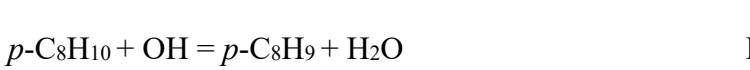

p-C_8H_{10} + OH = *p*-C_8H_9 + H_2O R6

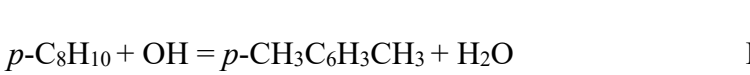

p-C_8H_{10} + OH = *p*-$CH_3C_6H_3CH_3$ + H_2O R7

p-C_8H_{10} + O = *p*-C_8H_9 + OH R8

p-C_8H_{10} + O = p-$CH_3C_6H_3CH_3$ + OH R9

p-C_8H_{10} + HO_2 = p-C_8H_9 + H_2O_2 R10

p-C_8H_{10} + HO_2 = p-$CH_3C_6H_3CH_3$ + H_2O_2 R11

p-C_8H_{10} + H = $A1CH_3$ + CH_3 R12

p-C_8H_{10} + OH = $HOC_6H_4CH_3$ + CH_3 R13

Previous theoretical and experimental studies [34-36] indicated that *p*-xylyl can undergo various decomposition reactions, including the unimolecular decomposition to *p*-xylylene (*p*-C_8H_8) (R14) or 3-methylfulvenallene (*m*-$C_7H_5CH_3$) (R15), the removal of the methyl group forming fulvenallene (C_7H_6) (R16), the ring contraction producing methylcyclopentadienyl ($C_5H_4CH_3$) (R17), and the isomerization to *o*-xylyl (*o*-C_8H_9) (R18), *m*-xylyl (*m*-C_8H_9) (R19) or *p*-dimethylphenyl (R20). Due to the lack of available rate coefficients for most of these reactions, previous kinetic models of *p*-xylene generally adopted an overall decomposition pathway of *p*-xylyl [11]. In the present model, pressure-dependent rate coefficients of these unimolecular reactions of *p*-xylyl were obtained with details shown in the annotation of Table S1.

p-C_8H_9 = p-C_8H_8 + H R14

p-C_8H_9 = m-$C_7H_5CH_3$ + H R15

p-C_8H_9 = C_7H_6 + CH_3 R16

p-C_8H_9 = $C_5H_4CH_3$ + C_2H_2 R17

p-C_8H_9 = o-C_8H_9 R18

m-C_8H_9 = p-C_8H_9 R19

p-$CH_3C_6H_3CH_3$ = p-C_8H_9 R20

Further decomposition pathways of their products, such as methylphenyl, toluene, fulvenallene, and methylcyclopentadienyl, have been introduced in detail in our previous models of aromatic fuels

[12, 26, 27, 37, 38]. As a resonantly stabilized radical, *p*-xylyl can also suffer the combination reactions with methyl (CH_3) (R21), benzyl (R22), and itself (R23).

$$p\text{-}CH_3C_6H_4C_2H_5 = p\text{-}C_8H_9 + CH_3 \quad \text{R21}$$

$$\text{bibenzyl-}CH_3 = p\text{-}C_8H_9 + A1CH_2 \quad \text{R22}$$

$$\text{dipxylyl} = p\text{-}C_8H_9 + p\text{-}C_8H_9 \quad \text{R23}$$

For the oxidation pathways of *p*-xylyl, special attention was paid to the formation pathways of several oxygenated aromatic intermediates including *p*-methylbenzaldehyde (*p*-$CH_3C_6H_4CHO$), *p*-cresol and *p*-hydroxybenzaldehyde (*p*-HOC_6H_4CHO). The reactions of *p*-xylyl with O or HO_2 can produce *p*-methylbenzaldehyde through *p*-methylbenzyloxy (*p*-$CH_3C_6H_4CH_2O$) (R24-R26).

$$p\text{-}C_8H_9 + O = p\text{-}CH_3C_6H_4CH_2O \quad \text{R24}$$

$$p\text{-}C_8H_9 + HO_2 = p\text{-}CH_3C_6H_4CH_2O + OH \quad \text{R25}$$

$$p\text{-}CH_3C_6H_4CH_2O = p\text{-}CH_3C_6H_4CHO + H \quad \text{R26}$$

p-Methylbenzaldehyde subsequently reacts with OH yielding *p*-methylbenzoyl (*p*-$CH_3C_6H_4CO$) (R27), which proceeds with decarbonylation to form methylphenyl (R28). Methylphenyl can add an O atom to form methylphenoxyl ($OC_6H_4CH_3$) (R29), eventually leading to *p*-cresol following the recombination reaction with H atom (R30).

$$p\text{-}CH_3C_6H_4CHO + OH = p\text{-}CH_3C_6H_4CO + H_2O \quad \text{R27}$$

$$p\text{-}CH_3C_6H_4CO = C_6H_4CH_3 + CO \quad \text{R28}$$

$$C_6H_4CH_3 + O = OC_6H_4CH_3 \quad \text{R29}$$

$$OC_6H_4CH_3 + H(+M) = HOC_6H_4CH_3(+M) \quad \text{R30}$$

Further H-loss of *p*-cresol at the methyl site produces *p*-hydroxylbenzyl ($HOC_6H_4CH_2$) (R31), which further reacts with O_2 to produce *p*-hydroxybenzyloxy ($HOC_6H_4CH_2O$) (R32) and ultimately decomposes to *p*-hydroxybenzaldehyde (R33).

$HOC_6H_4CH_2 + H = HOC_6H_4CH_3$ R31

$HOC_6H_4CH_2 + O_2 = HOC_6H_4CH_2O + O$ R32

$HOC_6H_4CH_2O = HOC_6H_4CHO + H$ R33

For *p*-hydroxybenzaldehyde, it can react with H, O and OH radicals forming *p*-hydroxybenzoyl (*p*-HOC_6H_4CO) (R34-R36), which in turn decomposes into phenoxy (A1O) and CO (R37).

$HOC_6H_4CHO + H = HOC_6H_4CO + H_2$ R34

$HOC_6H_4CHO + O = HOC_6H_4CO + OH$ R35

$HOC_6H_4CHO + OH = HOC_6H_4CO + H_2O$ R36

$HOC_6H_4CO = A1O + CO$ R37

The low-temperature oxidation reactions of *p*-xylyl were also incorporated in the present model. The addition of O_2 to the radical site of *p*-xylyl leads to *p*-xylyl peroxyl radical (R38), which subsequently reacts with HO_2 giving rise to *p*-xylyl hydroperoxide (*p*-$CH_3C_6H_4CH_2OOH$) (R39). Another route to the formation of *p*-xylyl hydroperoxide is the direct recombination of *p*-xylyl with HO_2 radical (R40). The fate of *p*-xylyl hydroperoxide involves a facile O-O bond scission, resulting in the formation of *p*-methylbenzyloxy and OH (R41).

p-$CH_3C_6H_4CH_2OO$ (+M) = *p*-C_8H_9 + O_2 (+M) R38

p-$CH_3C_6H_4CH_2OO + HO_2$ = *p*-$CH_3C_6H_4CH_2OOH + O_2$ R39

p-$C_8H_9 + HO_2$ = *p*-$CH_3C_6H_4CH_2OOH$ R40

p-$CH_3C_6H_4CH_2OOH$ = *p*-$CH_3C_6H_4CH_2O + OH$ R41

Note that the rate coefficients of R1-R41, including the reference reactions used for rate estimation, are listed in Table S1 and the details are provided in its annotations. Thermodynamic data of species in the *p*-xylene sub-mechanism were either taken from previous xylene models [7, 11, 18, 34] or calculated with the group additivity method by using the Therm software [39]. The calculation

uncertainties of the enthalpy of formation are generally about 2 kcal/mol for molecules and 4 kcal/mol for radicals [40]. The simulations of flow reactor pyrolysis and JSR oxidation were performed with the modules of Plug Flow Reactor and Perfectly Stirred Reactor in the Chemkin-Pro software [41], respectively. Besides the new data acquired in this work, the model was also validated against the available speciation data from the JSR oxidation of *p*-xylene at atmospheric pressure [11], the flow reactor oxidation at atmospheric pressure [10], and the low-pressure laminar premixed flames [12], and global combustion parameters including the ignition delay times [7, 15] and the laminar burning velocities [16, 18]. Table 1 summarizes the literature data for validation of the present model. Comparisons of simulated results with previous experimental data are shown in Figs. S1-S11 in the *Supplementary Materials.* The reaction mechanism, thermodynamic data, and transport data files are provided in the *Supplementary Materials*, while the chemical structures of species mentioned in this work are listed in Table S2 in the *Supplementary Materials*.

4. Results and discussion

In the following sections, the flow reactor pyrolysis results will be discussed first with special attention on the decomposition pathways of *p*-xylyl and the fuel-specific PAHs formation pathways. Subsequently, the JSR oxidation results will be discussed with special attention on the oxidation pathways of the fuel and key intermediates. Finally, the pyrolysis and oxidation of *p*-xylene will be compared with those of other two C_8H_{10} isomers (*o*-xylene and ethylbenzene) to explore the effects of fuel molecular structures on the combustion chemistry of C_8H_{10} isomers.

4.1. Flow reactor pyrolysis

4.1.1. Decomposition of p-xylene

Dozens of products were detected and identified in the pyrolysis of *p*-xylene, including radicals, isomers, and PAHs. A typical mass spectrum is provided in Fig. S12. Figure 1 presents experimental

and simulated mole fraction profiles of *p*-xylene and C_8-C_7 intermediates in the pyrolysis of *p*-xylene at 0.04-1 atm. The formation temperatures of *p*-xylyl (Fig. 1(b)) and toluene (Fig. 1(e)) are close to the decomposition temperature of fuel under all investigated pressures, indicating that they are the primary decomposition products of *p*-xylene. Styrene ($A1C_2H_3$) (Fig. 1(d)), benzyl (Fig. 1(f)), and fulvenallene (Fig. 1(g)) are generally formed at higher temperatures. Additionally, it is observed that *p*-xylylene (Fig. 1(c)), styrene, and toluene exhibit higher yields under all the investigated pressures, demonstrating that their formation pathways are less influenced by pressure and serve as dominant routes in the pyrolysis of *p*-xylene. In contrast, the concentration levels of free radical products such as benzyl and *p*-xylyl are relatively lower, ultimately leading to limited formation of fulvenallene and *p*-methylethylbenzene (Fig. 1(h)). This is due to the fact that fulvenallene and *p*-methylethylbenzene are mainly formed through the subsequent decomposition of benzyl and the recombination reaction of *p*-xylyl, respectively. To reveal the major decomposition pathways of *p*-xylene, the ROP and sensitivity analyses based on the *p*-xylene model developed in this work were conducted at 1509 K, 0.04 atm, and 1362 K, 1 atm, which correspond to 70% conversion of *p*-xylene. The reaction scheme derived from the ROP analysis is summarized in Fig. 2.

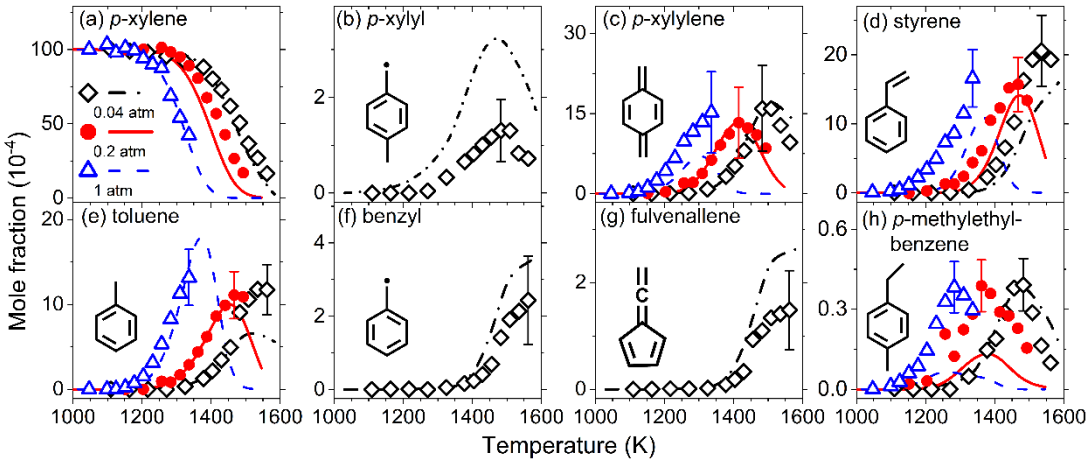

Fig. 1. Experimental (symbols) and simulated (lines) mole fraction profiles of *p*-xylene, *p*-xylyl, *p*-xylylene, styrene, toluene, benzyl, fulvenallene and *p*-methylethylbenzene in the flow reactor pyrolysis of *p*-xylene at 0.04, 0.2 and 1 atm.

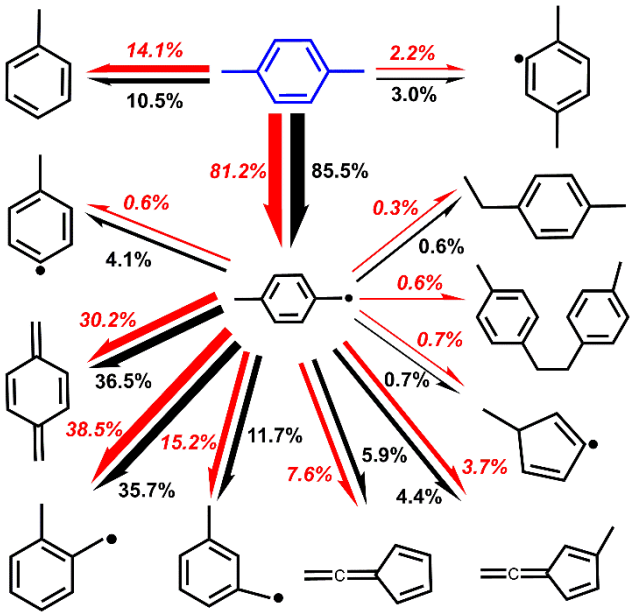

Fig. 2. Decomposition reaction network of *p*-xylene and *p*-xylyl in the pyrolysis of *p*-xylene at 0.04 and 1 atm. Black and red italic numbers (in percentage) beside the arrows denote the contributions of corresponding pathways weighted by the total consumption rates of reactants at 0.04 and 1 atm, respectively.

The ROP analysis of *p*-xylene shows that *p*-xylene is mainly converted to *p*-xylyl via the unimolecular decomposition (R1: *p*-C_8H_{10}(+M)=*p*-C_8H_9+H(+M)) and H-abstraction at the benzylic sites (R4: *p*-C_8H_{10}+H=*p*-C_8H_9+H_2), among which H-abstraction reactions dominate the consumption of *p*-xylene and their contribution becomes more significant with increasing pressure. Toluene is identified as the most abundant C_7 product in the pyrolysis of *p*-xylene with a peak mole fraction of 1.5×10^{-3} at 1 atm, as shown in Fig. 1(d). A large part of toluene is produced from the *ipso*-substitution reaction of *p*-xylene by the H atom (R12: *p*-C_8H_{10}+H=A1CH_3+CH_3). The sensitivity analysis of *p*-xylene in Fig. 3 also supports the key role of these reactions in the consumption of *p*-xylene. At 0.04 atm, the unimolecular decomposition and H-abstraction of *p*-xylene at the benzylic sites are the top two sensitive reactions with negative values. The sensitivity coefficient of the *ipso*-substitution reaction of *p*-xylene by the H atom greatly increases at 1 atm, while that of unimolecular decomposition noticeably decreases. The initial decomposition pathways of *p*-xylene at various

pressures are very similar to those in the flow reactor pyrolysis of toluene investigated by our group [26]. In particular, the consumption of both fuels is controlled by the unimolecular decomposition and H-atom abstraction reactions on the benzylic sites.

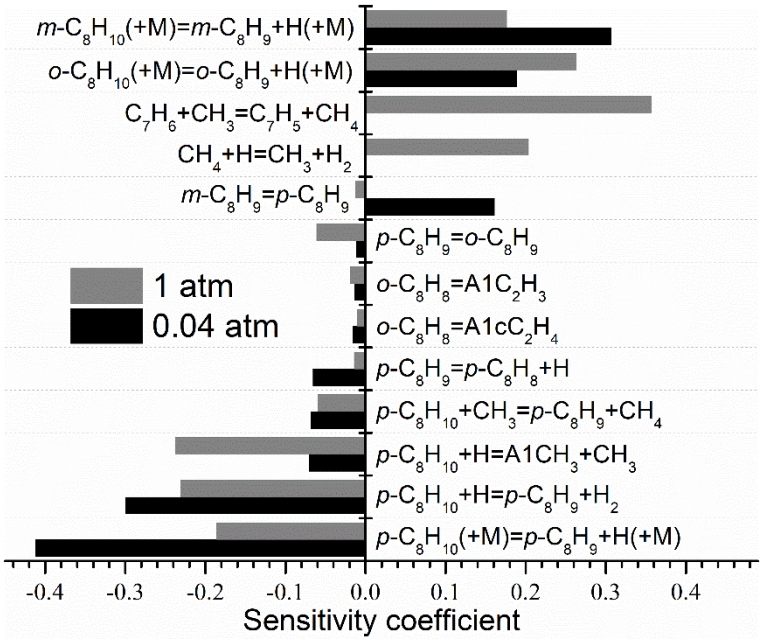

Fig. 3. Sensitivity analysis of *p*-xylene in the pyrolysis of *p*-xylene at 0.04 and 1 atm.

4.1.2. Consumption of p-xylyl radical

p-Xylyl has some similar decomposition pathways to benzyl [28], such as methylfulvenallene + H (R15: *p*-C_8H_9 = *m*-$C_7H_5CH_3$ + H), and methylcyclopentadienyl + acetylene (R17: *p*-C_8H_9 = $C_5H_4CH_3$ + C_2H_2). However, these pathways only play minor roles in the consumption of *p*-xylyl, as shown in Fig. 2. Instead, *p*-xylyl is mainly consumed through some specific reaction pathways. Among its decomposition pathways, the H-loss reaction from the remaining methyl group leads to the production of a resonantly stabilized molecule *p*-xylylene (R14: *p*-C_8H_9 = *p*-C_8H_8 + H). The contribution of this reaction to the consumption of *p*-xylyl exceeds 30% under all pressures. In addition, *p*-xylyl can also decompose to produce fulvenallene + CH_3 (R16: *p*-C_8H_9=C_7H_6+CH_3), which contributes less than 10% to *p*-xylyl consumption.

Another major consumption pathway of *p*-xylyl is the isomerization reaction. Three xylyl isomers (*p*-xylyl, *o*-xylyl, and *m*-xylyl) can isomerize with each other via the Ring-Contraction/Methylene-Migration (RCMM) mechanism. Isomeric reactions among the three xylyl radicals and their subsequent decomposition pathways are illustrated in Fig. S13. Based on the ROP analysis for *p*-xylyl, the isomerization of *p*-xylyl to *m*-xylyl (R19: *m*-C_8H_9=*p*-C_8H_9) only accounts for about 1/3 to 1/2 of that to *o*-xylyl (R18: *p*-C_8H_9=*o*-C_8H_9). The preference for R18 can be explained by the fact that *m*-xylyl is unable to decompose to *m*-xylylene [42]. In this work, two xylyl radicals (*p*-xylyl, *m*-xylyl), *o*-xylylene (*o*-C_8H_8), *p*-xylylene, and styrene were observed and identified by the PIE spectra of m/z = 105 and 104, as shown in Fig. S14 in *Supplementary Materials*. The observations provide evidence that *p*-xylyl does isomerize to *o*- and *m*-xylyl radicals [42].

Besides, the self-combination reaction of *p*-xylyl (R23: dipxylyl=*p*-C_8H_9+*p*-C_8H_9) and the combination reaction of *p*-xylyl with CH_3 (R21: *p*-$CH_3C_6H_4C_2H_5$=*p*-C_8H_9+CH_3) can also contribute to the consumption of *p*-xylyl. Different from the great contribution of similar reactions to benzyl consumption in the pyrolysis of toluene, the two combination reactions only have a little contribution (less than 1% even at 1 atm) due to the steric hindrance effect of *p*-xylyl.

p-Xylylene is a key intermediate that has a biradical feature [43] and its profiles (Fig. 1(c)) are captured by the present kinetic model. Compared with *o*-xylylene, *p*-xylylene is much more stable [44]. Therefore, the amount of *p*-xylylene produced in the pyrolysis of *p*-xylene is notably higher than that of *o*-xylylene formed in the pyrolysis of *o*-xylene [27]. Moreover, according to the work of Hirsch et al. [44], *p*-xylylene cannot isomerize to styrene or *o*-xylylene even at high temperatures. However, in the pyrolysis of *o*-xylene, styrene can be produced via either the direct isomerization reaction of *o*-xylylene (*o*-C_8H_8 = $A1C_2H_3$) or the sequential isomerization reaction through benzocyclobutene ($A1cC_2H_4$) (*o*-C_8H_8 = $A1cC_2H_4$ and $A1cC_2H_4$ = $A1C_2H_3$). Consequently, the concentration of styrene

(Fig. 1(d)) produced in the pyrolysis of *p*-xylene is lower than that in the pyrolysis of *o*-xylene under the same condition [27]. In the pyrolysis of *p*-xylene, styrene is also exclusively produced via these two pathways, but *o*-xylyl is produced from the isomerization reaction of *p*-xylyl instead of the consumption of *o*-xylene. Here the isomerization reactions among the three xylyl radicals are again emphasized for the species distribution in the high-temperature pyrolysis of *p*-xylene.

4.1.3. Formation of C_8-C_1 intermediates

Figure 4 shows experimental and simulated mole fraction profiles of C_8-C_1 intermediates observed in the pyrolysis of *p*-xylene. These species are mainly formed from the further decomposition of the primary decomposition products of *p*-xylene, i.e. *p*-xylyl, toluene and styrene. As displayed in Fig. 4(b), benzene (A1) is always of the highest concentration among all C_6 intermediates in the pyrolysis of *p*-xylene under various pressures, with a peak mole fraction of the magnitude of 10^{-3}. ROP analysis for benzene reveals that benzene is mainly produced from the unimolecular decomposition of styrene ($A1C_2H_3 = A1 + H_2CC$), the *ipso*-substitution reaction of styrene by H ($A1C_2H_3 + H = A1 + C_2H_3$), and the *ipso*-substitution reaction of toluene by H ($A1CH_3 + H = A1 + CH_3$). As the pressure increases, the contribution of unimolecular decomposition reaction to the production of benzene decreases, while the *ipso*-substitution reactions particularly that of toluene begin to play a leading role in benzene formation. In comparison with the pyrolysis of *o*-xylene under similar conditions [27], the maximum mole fractions of benzene observed in the pyrolysis of *p*-xylene are remarkably higher. This can be generally explained by the abundant production of toluene (Fig. 1(e)) in the pyrolysis of *p*-xylene.

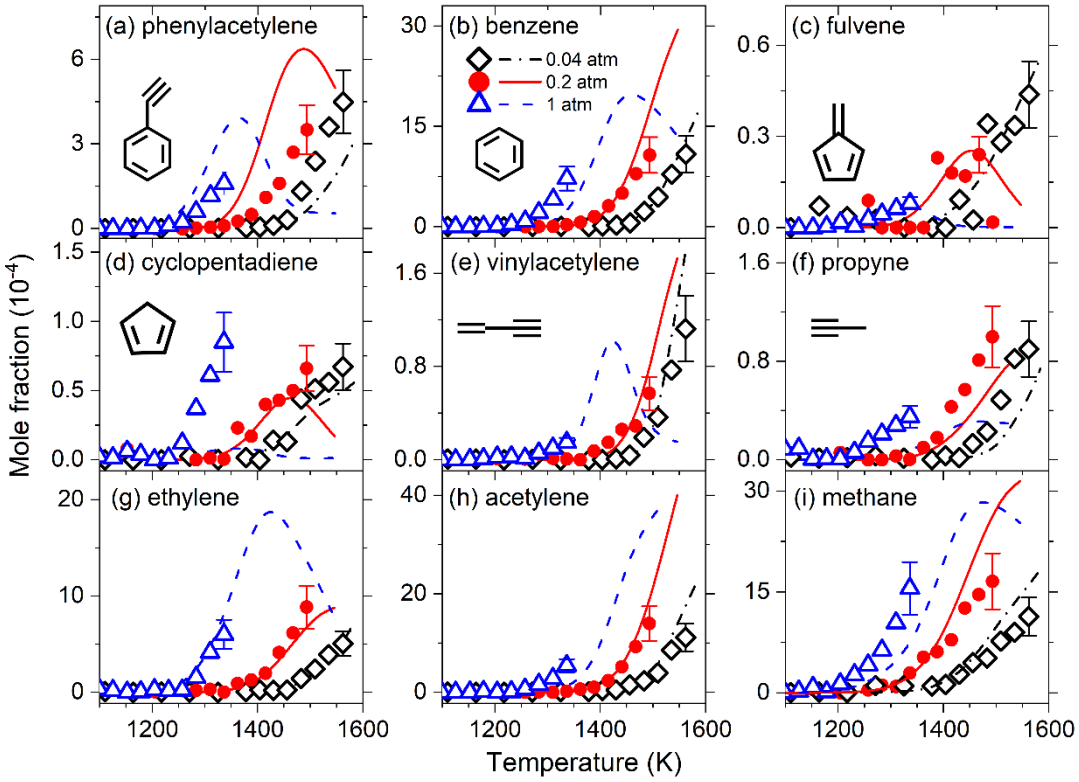

Fig. 4. Experimental (symbols) and simulated (lines) mole fraction profiles of phenylacetylene, benzene, fulvene, 1,3-cyclopentadiene, vinylacetylene, propyne, ethylene, acetylene and methane in the pyrolysis of *p*-xylene at 0.04, 0.2, and 1 atm.

Furthermore, the vinyl group attached to the benzenoid ring of styrene tends to undergo stepwise H-abstraction reactions, consequently leading to the formation of phenylacetylene (A1C$_2$H) (Fig. 4(a)). Other smaller products including 1,3-cyclopentadiene (C_5H_6) (Fig. 4(d)), vinylacetylene (C_4H_4) (Fig. 4(e)), and acetylene (Fig. 4(h)) mainly derive from the direct decomposition of *p*-xylyl, styrene, and fulvenallene, respectively, while the formation of propyne (pC_3H_4) (Fig. 4(f)) and methane (Fig. 4(i)) originates from a large number of H-abstraction reactions of propargyl and methyl radicals.

4.1.4. Formation and growth of PAHs

Figure 5 displays the experimental and simulated mole fraction profiles of typical bicyclic, tricyclic, and tetracyclic PAHs observed in this work. Based on the ROP analysis, the main formation pathways of major PAHs are summarized in Fig. 6. Indene (C_9H_8) (Fig. 5(b)) and naphthalene (A2) (Fig. 5(c)), which are the simplest bicyclic PAH species with fused ring structures, have significantly

higher concentrations than other PAH species, except for phenanthrene (A3) (Fig. 5(g)). It is found that the addition of CH_3 to vinylphenyl ($C_6H_4C_2H_3$), which is formed primarily by the dehydrogenation of styrene, dominates the production of indene with a contribution of more than 90% at 0.04 atm. However, at atmospheric pressure, the reaction $A1CH_2 + C_2H_2$ dominates indene formation. Other pathways with less contribution (<5%) to indene formation [29, 32] include the addition of propyne to benzyne (o-C_6H_4), the addition of ethylene (C_2H_4) to fulvenallenyl (C_7H_5), and the addition of CH_3 to phenylacetylene.

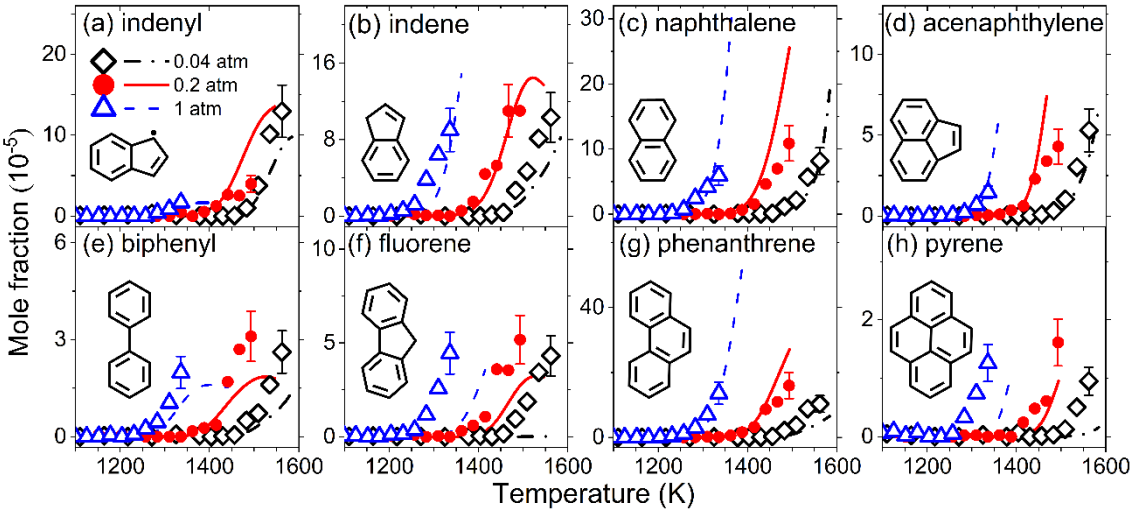

Fig. 5. Experimental (symbols) and simulated (lines) mole fraction profiles of indenyl, indene, naphthalene, acenaphthylene, biphenyl, fluorene, phenanthrene and pyrene in the pyrolysis of *p*-xylene at 0.04, 0.2, and 1 atm.

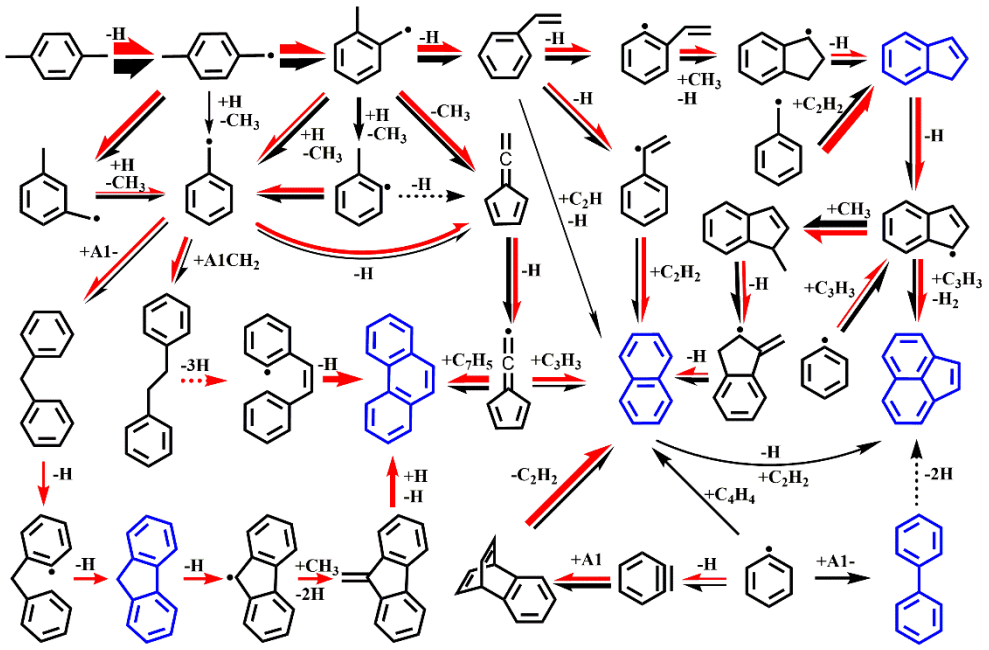

Fig. 6. Main reaction network of PAHs formation in the pyrolysis of *p*-xylene. The black and red arrows denote pathways at 0.04 and 1 atm, respectively. The species shown in blue color represent the PAH products observed in this work. Dotted arrows represent reaction pathways that need multiple steps to complete.

As for the consumption of indene, the removal of an H atom from the sp^3-hybridized carbon in the five-membered ring of indene forming indenyl (C_9H_7) is preferred. Indenyl (Fig. 5(a)) is the largest radical species detected in this experiment, which agrees with the measurements in the pyrolysis of toluene [26] and *o*-xylene [27]. The dehydrogenation and H-abstraction of indene are major reaction pathways contributing to indenyl production at 0.2 and 1 atm, while at 0.04 atm, indenyl is mainly formed via the addition of C_3H_3 to phenyl radical (A1-). The high concentration level of indenyl makes it play an important role in the formation of acenaphthylene (A2R5) (Fig. 5(d)), which is a typical cyclopenta-fused tricyclic PAH. The addition of C_3H_3 to indenyl contributes over 70% to A2R5 formation at all investigated pressures. Besides C_3H_3, indenyl can also combine with CH_3, resulting in the formation of 1-methylindene ($C_9H_7CH_3$), which is also an important consumption pathway of indenyl.

Various reaction pathways can contribute to the formation of naphthalene (Fig. 5(c)) [29, 30, 32]. At 0.04 atm, naphthalene is mainly derived from the addition of fulvenallenyl and C_3H_3, while the unimolecular decomposition of benzobicyclo[2, 2, 2]-octatriene (BICYCLO) [45] dominates when the pressure goes up to 1 atm. BICYCLO itself is a PAH produced from the radical/π-bond addition reaction between benzene and *o*-benzyne. The parent bicyclic moiety of BICYCLO was found prone to undergo bond cleavage to form naphthalene by elimination of acetylene. Besides the above-mentioned pathways, a small fraction of naphthalene can be also produced through the dehydrogenation and further ring rearrangement of 1-methylene-indan-2-yl radical ($C_9H_7CH_2$), the combination of 1-phenylvinyl and acetylene, and the addition of C_2H to styrene.

Phenanthrene (Fig. 5(g)) is the most abundant tricyclic PAH product observed in the pyrolysis of *p*-xylene and its formation mechanism [46-49] is more complicated than those yielding indene and naphthalene. As observed in Fig. 5(g), the present model can well capture the formation of phenanthrene at all pressures. ROP analysis for phenanthrene indicates that the self-combination reaction of fulvenallenyl is the dominant pathway leading to the formation of phenanthrene at 0.04 atm. At 1 atm, the H-loss in bibenzyl ($C_{14}H_{14}$), together with the subsequent cyclization process, facilitate the formation of phenanthrene to the maximum extent. It should be noted that both fulvenallenyl and bibenzyl can originate from benzyl, i.e., the unimolecular decomposition and self-combination reactions of benzyl lead to fulvenallenyl and bibenzyl, respectively. Here, we emphasize the crucial role of resonantly-stabilized radicals such as benzyl and fulvenallenyl in the formation of bicyclic and tricyclic PAHs including indene, naphthalene and phenanthrene, as illustrated in Fig. 6. Other pathways contributing to phenanthrene formation include the rearrangement reaction of hydro-methylenefluorene radical ($C_{13}H_9CH_2$) and the addition reaction of phenyl and phenylacetylene. Similar to 1-methylene-indan-2-yl radical, hydro-methylenefluorene radical is mainly formed through

the addition reaction of CH_3 to fluorenyl ($C_{13}H_9$). Fluorenyl mainly comes from the H-loss reaction of fluorene ($C_{13}H_{10}$), which is another fused tricyclic PAH with a 5-numbered ring observed in this work and presented in Fig. 5(f). Based on ROP analysis, fluorene is mainly produced through the addition reaction of phenyl to benzyl radical, followed by the H-loss and ring-closure reactions.

4.2. JSR oxidation

4.2.1. Consumption of p-xylene

Figures 7 and 8 display the experimental and simulated mole fraction profiles of *p*-xylene, O_2, major products (CO and CO_2), and aromatics produced in the JSR oxidation of *p*-xylene at 10 atm, τ = 0.5 s and ϕ = 0.5, 1.0 and 2.0. To reveal the key reactions in terms of fuel oxidation and major species formation, ROP analysis based on the *p*-xylene model developed in this work was performed at 950 K, 1010 K, and 1050 K for ϕ = 0.5, 1.0, and 2.0, respectively. It should be noted that the major pathways for the oxidation of the fuel and the formation of oxidation products are very close at different equivalence ratios, while the reaction fluxes of major pathways slightly change. Therefore, the main reaction network based on the ROP analysis results at ϕ = 1.0 is shown in Fig. 9 with special attention paid to the formation of oxygenated aromatic products.

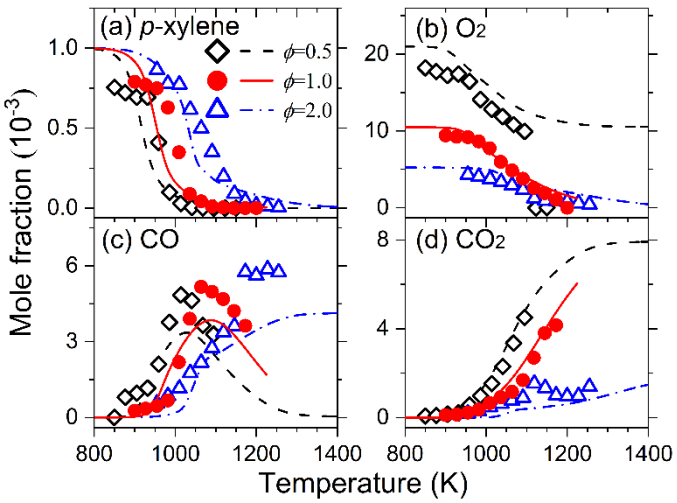

Fig. 7. Experimental (symbols) and simulated (lines) mole fraction profiles of *p*-xylene, oxygen, carbon monoxide, and carbon dioxide in the JSR oxidation of *p*-xylene at 10 atm, τ = 0.5 s and ϕ = 0.5, 1.0, and 2.0.

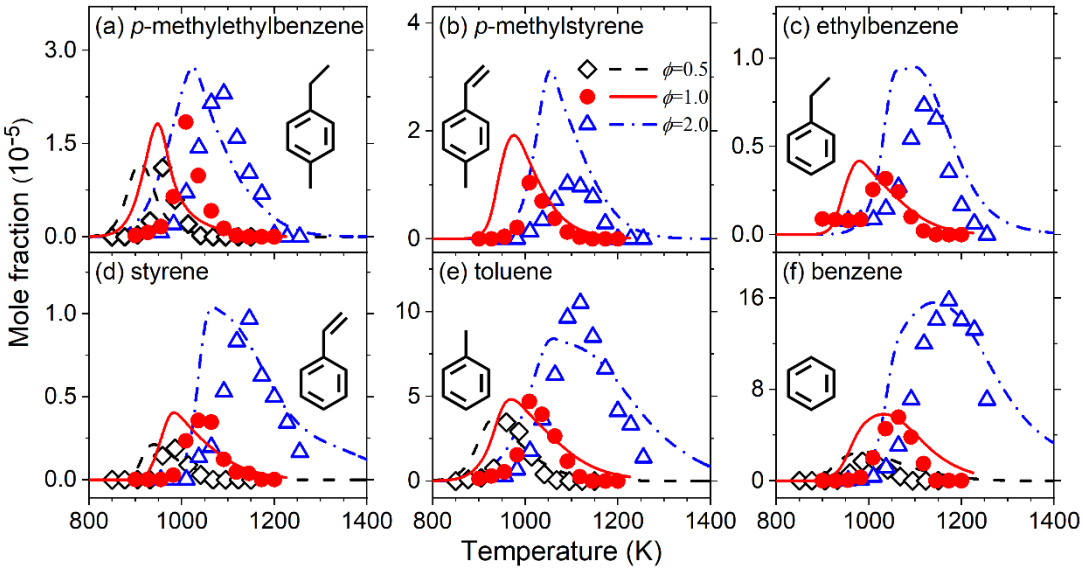

Fig. 8. Experimental (symbols) and simulated (lines) mole fraction profiles of *p*-methylethylbenzene, *p*-methylstyrene, ethylbenzene, styrene, toluene and benzene in the JSR oxidation of *p*-xylene at 10 atm, τ = 0.5 s and ϕ = 0.5, 1.0, and 2.0.

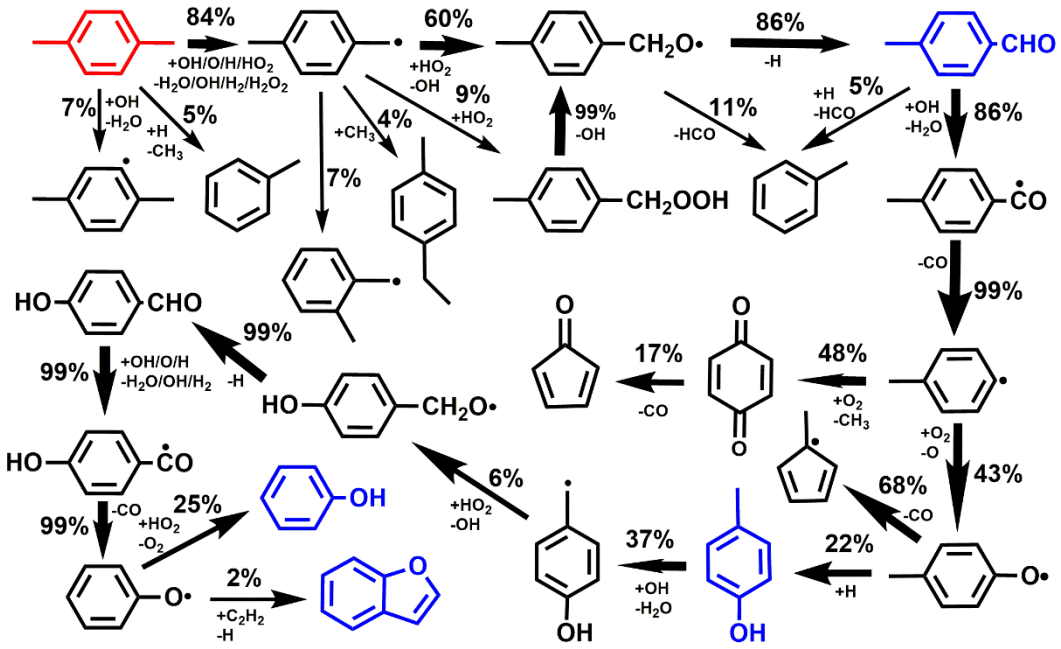

Fig. 9. Main reaction network concerning the formation of major oxygenated aromatic products in the JSR oxidation of *p*-xylene at 10 atm, τ = 0.5 s and ϕ = 1.0. The species shown in blue color represent the oxygenated aromatic products observed in this work.

As the equivalence ratio decreases from 2.0 to 0.5, H-abstraction reactions become increasingly important to fuel consumption, leading to a lower initial reaction temperature of *p*-xylene. ROP analysis for *p*-xylene shows that the contribution of H-abstraction reactions to fuel consumption is increased from 80% to 95% when switching from fuel-rich to fuel-lean conditions. These H-abstraction reactions mainly occur on the benzylic and phenylic sites of *p*-xylene by OH, O, and HO_2 radicals to produce *p*-xylyl (R6, R8, R10) and *p*-dimethylphenyl (R7, R9, R11), respectively. It should be noted that the contribution of unimolecular decomposition to the consumption of *p*-xylene (R1-R3) is extremely weak, even under fuel-rich condition. Another pathway that contributes to the *p*-xylene decay is the *ipso*-substitution reaction by H (R12: *p*-C_8H_{10}+H=A1CH_3+CH_3), especially under the fuel-rich condition where H concentration is higher.

The consumption pathways of *p*-xylyl significantly differ from those in the pyrolysis condition, among which the reaction with HO_2 plays a crucial role especially under fuel-lean condition. At ϕ = 0.5, around 70% of *p*-xylyl is oxidized by HO_2 leading to the production of *p*-methylbenzoxyl radical (R25: *p*-C_8H_9+HO_2=*p*-$CH_3C_6H_4CH_2O$+OH), while at ϕ = 2.0 this contribution decreases to around 30%. The isomerization reaction forming *o*-xylyl radical (R18: *p*-C_8H_9=*o*-C_8H_9) has an increasing contribution to *p*-xylyl consumption as the equivalence ratio raises (1% at ϕ = 0.5 and ~37% at ϕ = 2.0), thus competing with the reaction of *p*-xylyl with HO_2. The remaining small amount of *p*-xylyl undergoes combination reactions with CH_3 or HO_2 radicals to form *p*-methylethylbenzene (R21: *p*-$CH_3C_6H_4C_2H_5$=*p*-C_8H_9+CH_3) or *p*-xylyl hydroperoxide (R40: *p*-C_8H_9+HO_2=*p*-$CH_3C_6H_4CH_2OOH$), respectively, as shown in Fig. 9. It should be noted that some of the critical consumption pathways of

p-xylyl under pyrolysis conditions, such as the formation of *p*-xylylene (R14: *p*-C_8H_9=*p*-C_8H_8+H), fulvenallene (R16: *p*-C_8H_9=C_7H_6+CH_3), and methylfulvenallene (R15: *p*-C_8H_9=>*m*-$C_7H_5CH_3$+H), just have minor effects under oxidation conditions.

Benzene (Fig. 8(f)) is the most abundant aromatic product observed in the JSR oxidation of *p*-xylene. The maximum mole fraction of benzene at ϕ = 2.0 is around 2 times larger than that at ϕ = 0.5 and ϕ = 1.0, as seen in Fig. 8(f). ROP analysis for benzene indicates that the dominant formation pathway of benzene significantly differs at different equivalence ratios. At ϕ = 2.0, benzene formation is dominated by the concerted decarbonylation reaction of *o*-phthalaldehyde (*o*-$CHOC_6H_4CHO$) ($CHOC_6H_4CHO$ = A1 + 2CO). At ϕ = 0.5 and ϕ = 1.0, the concerted decarbonylation reaction of *o*-phthalaldehyde is not an important pathway, instead, benzene is mainly produced by the decarbonylation and ring-arrangement reactions of methylphenoxyl via the sequence of $OC_6H_4CH_3$ → $C_5H_4CH_3$ → fulvene → A1. Toluene (Fig. 8(e)) is the second most abundant aromatic product observed in the oxidation of *p*-xylene. The dominant formation pathway of toluene also varies with equivalence ratios. At ϕ = 2.0, toluene is mainly produced from the *ipso*-substitution reaction of *p*-xylene by H (R12: *p*-C_8H_{10}+H=$A1CH_3$+CH_3), while at ϕ = 0.5 and ϕ = 1.0, decomposition of *p*-methylbenzoxyl radical (*p*-$CH_3C_6H_4CH_2O$ = $A1CH_3$ + HCO) is the dominant reaction contributing to toluene formation.

In comparison to the abundant production of styrene in the pyrolysis of *p*-xylene (Fig. 1(d)), the importance of styrene is lowered under oxidation conditions (Fig. 8(d)). The produced *o*-xylylene, which comes from the reaction of *o*-xylyl with O_2 (*o*-C_8H_9 + O_2 = *o*-C_8H_8 + HO_2), is mainly converted to *o*-methylenebenzaldehyde (*o*-C_8H_8 + O_2 = *o*-$CH_2C_6H_4CHO$ + OH), rather than to styrene (*o*-C_8H_8 = $A1C_2H_3$). In fact, most styrene is produced from $A1C_2H_5$ either via the reaction sequence $A1C_2H_5$ → $A1CHCH_3$ → $A1C_2H_3$ or via $A1C_2H_5$ → $A1CH_2CH_2$ → $A1CH_2CH_2OO$ → $A1C_2H_3$. Under the fuel-

rich condition, the former pathway dominates styrene formation, while under the lean condition the latter pathway is dominant.

Ethylbenzene (Fig. 8(c)), *p*-methylethylbenzene (Fig. 8(a)), and *p*-methylstyrene (Fig. 8(b)) are three major secondary aromatic products produced through the addition reactions of benzyl or *p*-xylyl. For instance, ethylbenzene is exclusively produced from the addition of CH_3 to benzyl ($A1C_2H_5$ = $A1CH_2$ + CH_3), while *p*-methylethylbenzene is mainly derived from the addition of CH_3 to *p*-xylyl (R21: *p*-$CH_3C_6H_4C_2H_5$=*p*-C_8H_9+CH_3). The H-loss reactions of ethylbenzene and *p*-methylethylbenzene eventually lead to the formation of styrene and *p*-methylstyrene, respectively.

4.2.2. Formation of oxygenated aromatics

Figure 10 shows major oxygenated aromatics observed in the oxidation of *p*-xylene at three equivalence ratios. *p*-Methylbenzaldehyde (Fig. 10(a)) is the most abundant oxygenated aromatic because it is the major direct oxidation product of *p*-xylyl. As an unstable low-temperature intermediate, *p*-xylyl hydroperoxide (*p*-$CH_3C_6H_4CH_2OOH$), which originates from the addition reaction of *p*-xylyl with HO_2 (R40: *p*-C_8H_9+HO_2=*p*-$CH_3C_6H_4CH_2OOH$), quickly dissociates into *p*-methylbenzoxyl radical with the release of OH (R41: *p*-$CH_3C_6H_4CH_2OOH$=*p*-$CH_3C_6H_4CH_2O$+OH). *p*-Methylbenzoxyl radical loses an H atom resulting in the formation of *p*-methylbenzaldehyde (R26: *p*-$CH_3C_6H_4CH_2O$=*p*-$CH_3C_6H_4CHO$+H).

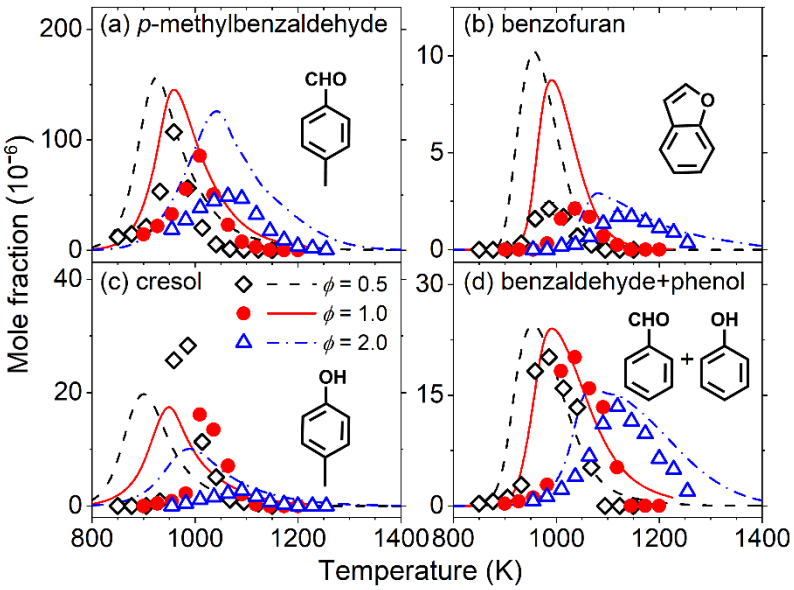

Fig. 10. Experimental (symbols) and simulated (lines) mole fraction profiles of *p*-methylbenzaldehyde, benzofuran, cresol and benzaldehyde plus phenol in the JSR oxidation of *p*-xylene at 10 atm, τ = 0.5 s and ϕ = 0.5, 1.0, and 2.0.

Decomposition reactions of *p*-methylbenzaldehyde provide essential precursors for the formation of other oxygenated aromatics, such as benzofuran (Fig. 10(b)) and cresol (Fig. 10(c)). The produced *p*-methylbenzaldehyde mainly undergoes H-atom abstraction reaction producing *p*-methylbenzoyl (R27: *p*-$CH_3C_6H_4CHO$+OH=*p*-$CH_3C_6H_4CO$+H_2O), which subsequently dissociates into methylphenyl via the decarbonylation reaction (R28: *p*-$CH_3C_6H_4CO$=$C_6H_4CH_3$+CO). A majority of methylphenyl undergoes the reaction with O_2 forming *p*-benzoquinone (*p*-$C_6H_4O_2$), and the rest is converted to methylphenoxyl (R29: $C_6H_4CH_3$+O=$OC_6H_4CH_3$). Methylphenoxyl tends to react via decarbonylation, producing methylcyclopentadienyl, or converts to cresol by adding an H atom (R30: $OC_6H_4CH_3$+H(+M)=$HOC_6H_4CH_3$(+M)). The conversion from cresol to *p*-hydroxybenzaldehyde (*p*-HOC_6H_4CHO) via R31-R33 is similar to the oxidation process of *p*-xylene to *p*-methylbenzaldehyde described above. *p*-Hydroxybenzaldehyde tends to proceed with H-atom abstraction reactions of R34-R36, followed by the decarbonylation process to form phenoxy radical (R37: HOC_6H_4CO=A1O+CO). Phenoxy radical can either be converted to phenol (A1OH) by recombining with an H-atom, or

undergo addition reaction with acetylene forming benzofuran (C_8H_6O). Note that the phenoxy + acetylene pathway contributes significantly to the formation of benzofuran, rendering it another typical product of the oxidation of *p*-xylene.

4.2.3. Formation of C_5-C_1 products

Figure 11 presents the experimental and simulated mole fraction profiles of typical C_5-C_1 products. 1,3-cyclopentadiene (Fig. 11(a)) and 1,3-butadiene (C_4H_6) (Fig. 11(b)) are significant C_5 and C_4 intermediates produced during the oxidation of *p*-xylene with close concentration levels. In comparison to *o*-xylene oxidation [27] under similar conditions, the maximum mole fraction of 1,3-cyclopentadiene is notably lower while the maximum mole fraction of 1,3-butadiene is similar in the oxidation of *p*-xylene. According to ROP analysis, the majority of 1,3-cyclopentadiene is produced from the oxidation reaction of phenol, while the formation of 1,3-butadiene is dominated by the reactions of 1,3-cyclopentadiene with O or OH. Vinylacetylene (C_4H_4) (Fig. 11(c)) is another important C_4 product observed here. The present model generally over-predicts its maximum mole fractions, especially under the fuel-rich condition. ROP analysis shows that vinylacetylene is mainly produced through the decarbonylation of cyclopentadienone (C_5H_4O), which is formed from phenol via the reaction sequence A1OH $\rightarrow$ C_6H_4OH $\rightarrow$ OC_6H_4OH $\rightarrow$ C_5H_4O. It should be noted that rate coefficients for the above reactions were generally estimated from similar reactions of benzene or phenoxy, which could explain the over-prediction of vinylacetylene. The formation of propene (Fig. 11(d)) is strongly related to allyl radical, which can be produced mainly by the decomposition of vinylacetylene. An over-prediction of propene under the fuel-rich condition can be also noticed in Fig. 11 (d).

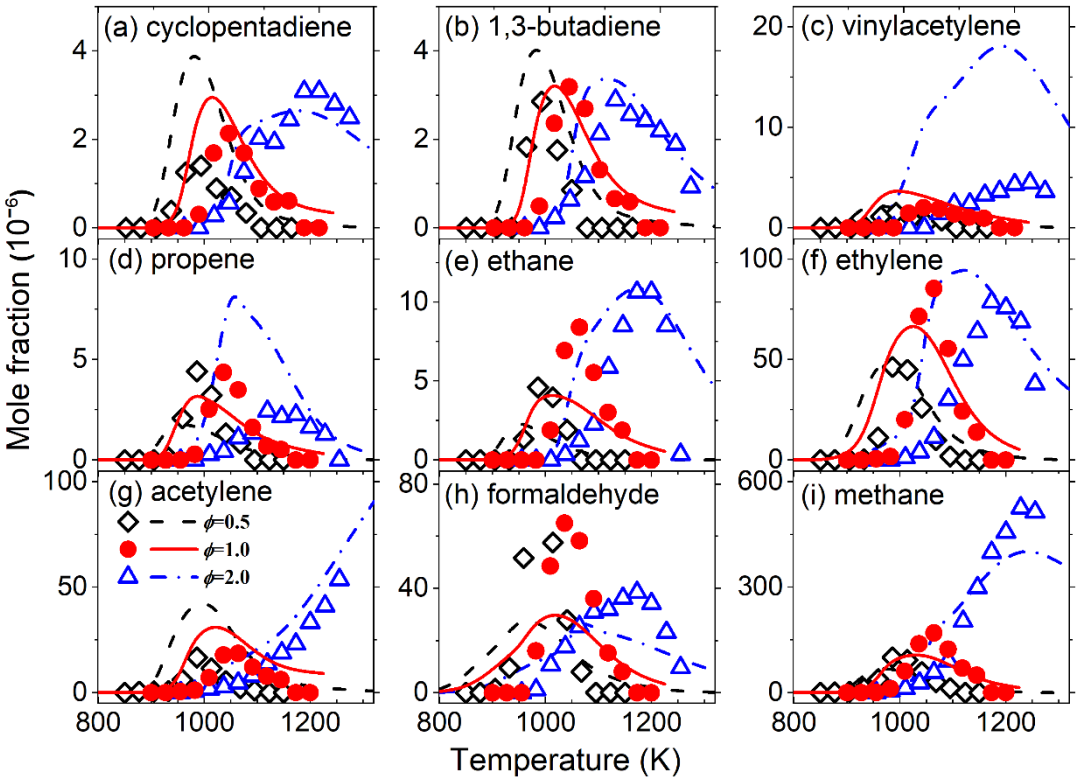

Fig. 11. Experimental (symbols) and simulated (lines) mole fraction profiles of 1,3-cyclopentadiene, 1,3-butadiene, vinylacetylene, propene, ethane, ethylene, acetylene, formaldehyde and methane in the JSR oxidation of *p*-xylene at 10 atm, τ = 0.5 s and ϕ = 0.5, 1.0, and 2.0.

Ethylene (Fig. 11(f)) and acetylene (Fig. 11(g)) are two major C_2 species produced during the oxidation of *p*-xylene. At ϕ = 0.5, ethylene is mainly produced from the reaction of acrolein (C_2H_3CHO) with OH, while at ϕ = 2.0, it is mainly produced from the H-loss reaction of ethyl (C_2H_5). The major formation pathway of acrolein is also related to C_5 species, i.e., via the reaction sequence $C_5H_4O \rightarrow$ *n*-$C_4H_5 \rightarrow C_2H_3CHO$. For acetylene, the major production pathways are similar at the three different equivalence ratios. Based on ROP analysis, acetylene is mainly produced from the oxidation reaction of *p*-benzoquinone and partly produced from the oxidation reaction of C_5H_3O, which derives from the H-loss of cyclopentadienone. Therefore, it can be concluded that C_5 chemistry plays a key role in the formation of C_5-C_2 species in the oxidation of *p*-xylene.

4.3 Comparison among the combustion chemistry of C_8H_{10} isomers

Xylene isomers and ethylbenzene are C_8H_{10} isomers that have different combustion chemistry

due to their different chemical structures. In previous work, Yuan et al. have investigated the combustion chemistry of ethylbenzene [38] and *o*-xylene [27] using methods similar to those in this work. In the following section, the combustion chemistry of *p*-xylene, *o*-xylene, and ethylbenzene are compared in terms of pyrolysis and oxidation reactivity of the fuels, and PAHs formation and growth.

4.3.1 Pyrolysis and oxidation reactivity of C_8H_{10} fuels

Figure 12(a) compares the experimental and simulated fuel consumption profiles during the pyrolysis of *p*-xylene, *o*-xylene, and ethylbenzene under the same condition (1 mol% fuel and 99 mol% Ar). The initial decomposition temperature of ethylbenzene is remarkably lower (approximately 250 K) than that of *p*-xylene and *o*-xylene, indicating that ethylbenzene has the highest pyrolysis reactivity among the three fuels. This can be explained by the weak benzylic C-C bond in ethylbenzene, which is easy to break under pyrolysis conditions.

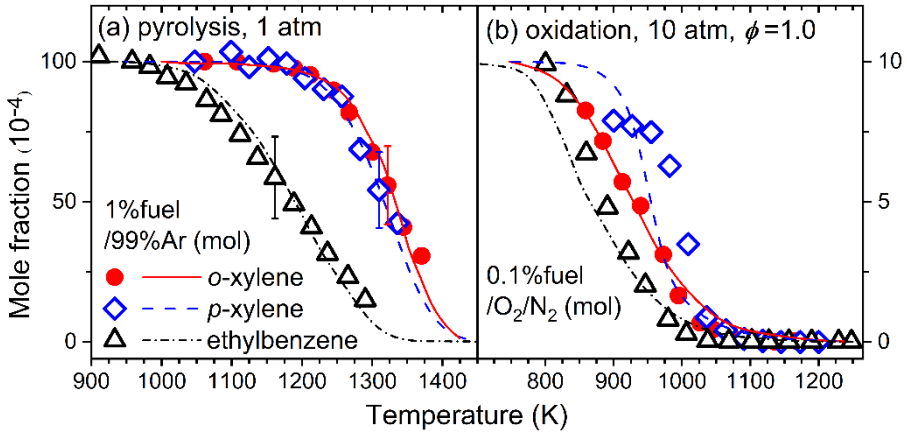

Fig. 12. Comparison of fuel reactivity of *p*-xylene, *o*-xylene [27], and ethylbenzene [38] in (a) flow reactor pyrolysis experiments at 1 atm; (b) JSR oxidation experiments at 10 atm, $\tau = 0.5$ s and $\phi = 1.0$.

The decomposition profile of *p*-xylene tends to shift towards lower temperatures than that of *o*-xylene, indicating that *p*-xylene has a slightly higher pyrolysis reactivity. It is generally accepted that the C-H bond dissociation on the methyl sidechain yielding xylyl radicals dominates the decomposition of *p*-xylene and *o*-xylene [13]. Da Costa et al. [50] determined the rate coefficients of

p-/*o*-C_8H_{10} (+M) = *p*-/*o*-C_8H_9 + H (+M) and concluded that the activation energies between them are identical within 2 kJ/mol. Hence, *p*-xylene and *o*-xylene showed almost identical decomposition rates. Apart from the C-H bond dissociation reactions of fuels, the subsequent scission reactions of *p*-xylyl or *o*-xylyl, i.e. *p*-/*o*-C_8H_9 = *p*-/*o*-C_8H_8 + H, also control fuel decomposition [27]. Fernandes et al. [14] measured the activation energies for the dissociation of *p*-xylyl and *o*-xylyl in a shock tube to be about 295 and 310 kJ/mol, respectively, which explains the slightly higher pyrolysis reactivity of *p*-xylene than that of *o*-xylene.

Regarding the fuel reactivity under oxidation conditions, experimental and simulated mole fraction profiles of *p*-xylene, *o*-xylene, and ethylbenzene in the JSR are compared under the same condition (0.1 mol% fuel/O_2/N_2, 10 atm, ϕ = 1.0) in Fig. 12(b). It can be seen that among the three C_8H_{10} isomers, ethylbenzene has the highest oxidation reactivity because the produced 1-phenylethyl radical is prone to undergo the intermediate temperature chain-branching oxidation reactions to facilitate the oxidation process, while such reactions involving alkylperoxy radical isomerization are not feasible for *p*-xylene and *o*-xylene, due to their shorter methyl side chain. As discussed in [38], over 90% of 1-phenylethyl is oxidized by O_2 to produce 1-phenylethylperoxy radical (A1CH(OO)CH_3), which indicates that an obvious low-temperature peroxy radical chemistry occurs in ethylbenzene oxidation at 10 atm, enhancing the low-temperature reactivity. Compared to *o*-xylene, *p*-xylene exhibits lower oxidation reactivity at lower temperatures, while at higher temperatures both show similar oxidation reactivity, which renders the temperature window of *p*-xylene oxidation narrower than that of *o*-xylene. Generally, this is caused by their fuel-isomeric effects. The *ortho*-effect of the adjacent methyl pairs presented in *o*-xylene and the possible formation of ketohydroperoxide species can promote the oxidation of *o*-xylene. As discussed in [27], the *ortho*-effect of *o*-xylene is mainly attributed to the chain-branching chemistry involved in the oxidation of *o*-xylyl, *o*-methylbenzoxyl, *o*-

methylphenyl and *o*-methylbenzylperoxide radicals. The adjacent sites on the benzenoid ring facilitate the intramolecular H-transfer and isomerization processes of these *ortho*-substituted benzylic type radicals. In conclusion, the differences in the pyrolysis reactivity of the three C_8H_{10} isomers can be attributed to variations in the activation energies of their primary decomposition pathways, while the discrepancies in their oxidation reactivity are determined by the unique chain branching chemistry in ethylbenzene and *ortho*-positioned chemistry specific to *o*-xylene.

4.3.2 PAHs formation and growth

Besides fuel reactivity, the formation and growth of PAHs are also of concern for fuel combustion characteristics, particularly for aromatic fuels. Figure 13 compares mole fraction profiles of typical PAHs, i.e., indene, naphthalene, and phenanthrene produced during the flow reactor pyrolysis of *p*-xylene, *o*-xylene, and ethylbenzene under the same condition (1 mol% fuel and 99 mol% Ar, 1atm). As can be observed, the concentration levels of three PAHs produced in the pyrolysis of *p*-xylene, *o*-xylene, and ethylbenzene are comparable. The initial formation temperatures of indene, naphthalene, and phenanthrene are generally lower in the pyrolysis of ethylbenzene than those in *p*-xylene and *o*-xylene pyrolysis. As for the two xylene isomers, the initial formation temperatures of indene and naphthalene in the pyrolysis of *o*-xylene are slightly lower than those in the pyrolysis of *p*-xylene, which is opposite to the trend of initial decomposition temperature of the fuels.

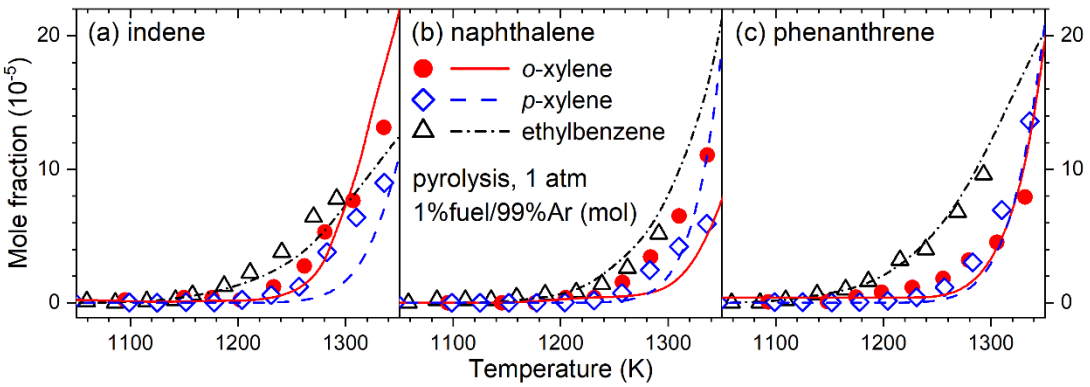

Fig. 13. Comparison of mole fraction profiles of indene, naphthalene, and phenanthrene in the flow reactor pyrolysis of *p*-xylene, *o*-xylene [27], and ethylbenzene [38] at 1 atm.

Nevertheless, the dominant formation pathways of indene and naphthalene are quite different, depending on the major precursors formed in the pyrolysis of the three C_8H_8 isomers. In the pyrolysis of ethylbenzene and *o*-xylene at 1 atm, indene is mainly produced via the addition reaction of CH_3 to vinylphenyl, whereas in the pyrolysis of *p*-xylene at 1 atm, indene is mainly produced by the addition reaction of acetylene to benzyl. This is because styrene as the precursor of vinylphenyl can be abundantly produced via the H-loss reaction of phenyethyl and *o*-xylyl in the pyrolysis of ethylbenzene and *o*-xylene, respectively. However, in the pyrolysis of *p*-xylene, styrene cannot be directly produced from the decomposition and isomerization of fuel radicals. In contrast, toluene is produced in large amounts in the pyrolysis of *p*-xylene via the *ipso*-substitution reaction, thus serving as a critical precursor of benzyl radical.

Regarding naphthalene, in the pyrolysis of ethylbenzene and *o*-xylene at 1 atm, it is mainly produced by the addition reaction of acetylene to 1-phenylvinyl ($A1CCH_2$), which is also produced through the H-loss reaction of styrene. In the pyrolysis of *p*-xylene, due to the easy benzene formation, naphthalene is mainly produced by the decomposition reaction of BICYCLO, which is produced through the radical/π-bond addition reaction between benzene and *o*-benzyne. The dominant formation pathways of phenanthrene are similar in the pyrolysis of three C_8H_{10} isomers, i.e., from benzyl via the reaction sequence $A1CH_2 \rightarrow C_{14}H_{14} \rightarrow C_{14}H_{13} \rightarrow C_{14}H_{12} \rightarrow C_{14}H_{11} \rightarrow$ A3. It is concluded that the lowest formation temperature of the three PAHs in the pyrolysis of ethylbenzene mainly results from its higher pyrolysis rate, while the lower formation temperatures of indene and naphthalene in the pyrolysis of *o*-xylene than those in the pyrolysis of *p*-xylene are associated to the more efficient formation of PAH precursors, especially styrene.

5. Conclusions

This work reports the pyrolysis of *p*-xylene in a flow reactor at various pressures from 0.04 to 1 atm and the oxidation of *p*-xylene in a JSR at 10 atm. A detailed kinetic model for *p*-xylene combustion over wide conditions (800-1600 K, 0.04-10 atm) was established and validated against extensive experimental datasets of *p*-xylene in this work and literature covering pyrolysis, oxidation, ignition, flame species and flame speeds. Overall, the kinetic model can reasonably capture the experimental data and thus can be further used for accurate modeling of surrogate fuels. Fingerprint intermediates and isomeric radicals like *p*-/*o*-/*m*-xylyls, benzyl, *p*-/*o*-xylylenes, styrene, benzene and fulvene, etc., were detected and successfully distinguished in the pyrolysis of *p*-xylene. *p*-Xylene decomposition was initiated via C-H bond dissociation at the methyl group to yield *p*-xylyl, which subsequently decomposes to *p*-xylylene or isomerizes to *o*- and *m*-xylyl. Typical PAHs species including indene, naphthalene, biphenyl, acenaphthylene, fluorene, phenanthrene, pyrene, etc., were also observed in *p*-xylene pyrolysis, and their major formation pathways at different pressures were elucidated. ROP analysis reveals that fulvenallenyl plays a crucial role in the formation of PAHs in *p*-xylene pyrolysis at 0.04 atm, while benzyl is the major precursor for the formation of PAHs at 1 atm. In the JSR oxidation of *p*-xylene, major oxygenated aromatics such as *p*-methylbenzaldehyde, cresol, and benzofuran were identified, emphasizing the high-pressure oxidation chemistry of *p*-xylene. *p*-Xylene is predominantly consumed via H-abstraction by OH, O, and HO_2 radicals forming *p*-xylyl, which is subsequently converted to *p*-methylbenzaldehyde.

The fuel-isomeric effects of *p*-xylene, *o*-xylene and ethylbenzene on their pyrolysis and oxidation reactivity, as well as on the formation kinetics of major PAH products, were emphasized in this work. The higher pyrolysis reactivity of ethylbenzene than *p*-xylene and *o*-xylene mainly arises from the weaker benzylic C-C bond in ethylbenzene. The higher oxidation reactivity of ethylbenzene than

xylenes is primarily attributed to the low-temperature reactions of fuel radical 1-phenylethyl, while the higher oxidation reactivity of *o*-xylene than *p*-xylene results from the *ortho*-effect. Regarding the formation of PAHs, the lower formation temperatures of indene, naphthalene, and phenanthrene in the pyrolysis of ethylbenzene mainly originate from its highest pyrolysis reactivity, while the lower formation temperatures of indene and naphthalene in the pyrolysis of *o*-xylene, in comparison to *p*-xylene, are associated to the more efficient formation of PAH precursors, especially styrene.

Acknowledgments

The authors are grateful for the funding support from the National Natural Science Foundation of China (52376119, 52206164), Science Center for Gas Turbine Project (P2022-B-II-0-017-001) and Oceanic Interdisciplinary Program of Shanghai Jiao Tong University (SL2022ZD104).

References

[1] L. Shafer, R. Striebich, J. Gomach, T. Edwards. Chemical class composition of commercial jet fuels and other specialty kerosene fuels. 14th AIAA/AHI space planes and hypersonic systems and technologies conference; 2006. p. 7972.
[2] H. Jin, W. Yuan, W. Li, J. Yang, Z. Zhou, L. Zhao, Y. Li, F. Qi, Combustion chemistry of aromatic hydrocarbons, Prog. Energy Combust. Sci. 96 (2023) 101076.
[3] W.J. Pitz, C.J. Mueller, Recent progress in the development of diesel surrogate fuels, Prog. Energy Combust. Sci. 37 (2011) 330-350.
[4] F.L. Dryer, Chemical kinetic and combustion characteristics of transportation fuels, Proc. Combust. Inst. 35 (2015) 117-144.
[5] S.M. Sarathy, A. Farooq, G.T. Kalghatgi, Recent progress in gasoline surrogate fuels, Prog. Energy Combust. Sci. 65 (2018) 67-108.
[6] S. Dooley, S.H. Won, F.L. Dryer, Surrogate fuels and combustion characteristics of liquid transportation fuels, Computer Aided Chemical Engineering, Elsevier2019, pp. 513-602.
[7] F. Battin‐Leclerc, R. Bounaceur, N. Belmekki, P. Glaude, Experimental and modeling study of the oxidation of xylenes, Int. J. Chem. Kinet. 38 (2006) 284-302.
[8] R.H. Natelson, M.S. Kurman, R.O. Johnson, N.P. Cernansky, D.L. Miller, Preignition and autoignition chemistry of the xylene isomers, Combust. Sci. Technol. 183 (2011) 897-914.
[9] W. Sun, A. Hamadi, F.E.C. Ardila, S. Abid, N. Chaumeix, A. Comandini, Insights into pyrolysis kinetics of xylene isomers behind reflected shock waves, Combust. Flame 244 (2022) 112247.
[10] J.L. Emdee, K. Brezinsky, I. Glassman, High-temperature oxidation mechanisms of *m*- and *p*-xylene, The Journal of Physical Chemistry 95 (1991) 1626-1635.
[11] S. Gaïl, P. Dagaut, Experimental kinetic study of the oxidation of p-xylene in a JSR and comprehensive detailed chemical kinetic modeling, Combust. Flame 141 (2005) 281-297.
[12] W.H. Yuan, L. Zhao, J.Z. Yang, Z.Y. Zhou, Y.Y. Li, F. Qi, Insights into the decomposition and oxidation chemistry of *p*-xylene in laminar premixed flames, J. Phys. Chem. A 125 (2021) 3189-3197.

[13] H. Hippler, S. Seisel, J. Troe, Pyrolysis of *p*-xylene and 4-methylbenzyl radicals, Proc. Combust. Inst. 25 (1994) 875-882.
[14] R.X. Fernandes, A. Gebert, H. Hippler, The pyrolysis of 2-, 3-, and 4-methylbenzyl radicals behind shock waves, Proc. Combust. Inst. 29 (2002) 1337-1343.
[15] H.-P.S. Shen, M.A. Oehlschlaeger, The autoignition of C_8H_{10} aromatics at moderate temperatures and elevated pressures, Combust. Flame 156 (2009) 1053-1062.
[16] C.S. Ji, E. Dames, H. Wang, F.N. Egolfopoulos, Propagation and extinction of benzene and alkylated benzene flames, Combust. Flame 159 (2012) 1070-1081.
[17] I. Meziane, N. Delort, O. Herbinet, R. Bounaceur, F. Battin-Leclerc, A comparative study of the oxidation of toluene and the three isomers of xylene, Combust. Flame 257 (2023) 113046.
[18] L. Dupont, H.Q. Do, G. Capriolo, A.A. Konnov, A. El Bakali, Experimental and kinetic modeling study of para-xylene chemistry in laminar premixed flames, Fuel 239 (2019) 814-829.
[19] G. Kukkadapu, D. Kang, S.W. Wagnon, K. Zhang, M. Mehl, M. Monge-Palacios, H. Wang, S.S. Goldsborough, C.K. Westbrook, W.J. Pitz, Kinetic modeling study of surrogate components for gasoline, jet and diesel fuels: C_7-C_{11} methylated aromatics, Proc. Combust. Inst. 37 (2019) 521-529.
[20] Z.Y. Zhou, M.F. Xie, Z.D. Wang, F. Qi, Determination of absolute photoionization cross‐sections of aromatics and aromatic derivatives, Rapid Commun. Mass Spectrom. 23 (2009) 3994-4002.
[21] Z.Y. Zhou, X.W. Du, J.Z. Yang, Y.Z. Wang, C.Y. Li, S. Wei, L.L. Du, Y.Y. Li, F. Qi, Q.P. Wang, The vacuum ultraviolet beamline/endstations at NSRL dedicated to combustion research, J. Synchrotron Radiat. 23 (2016) 1035-1045.
[22] C. Narayanan, S. Srinivasan, A.K. Datye, R. Gorte, A. Biaglow, The effect of alumina structure on surface sites for alcohol dehydration, J. Catal. 138 (1992) 659-674.
[23] P. Glarborg, P.G. Kristensen, S.H. Jensen, K. Dam-Johansen, A flow reactor study of HNCO oxidation chemistry, Combust. Flame 98 (1994) 241-258.
[24] P.G. Kristensen, P. Glarborg, K. Dam-Johansen, Nitrogen chemistry during burnout in fuel-staged combustion, Combust. Flame 107 (1996) 211-222.
[25] Y.J. Zhang, J.H. Cai, L. Zhao, J.Z. Yang, H.F. Jin, Z.J. Cheng, Y.Y. Li, L.D. Zhang, F. Qi, An experimental and kinetic modeling study of three butene isomers pyrolysis at low pressure, Combust. Flame 159 (2012) 905-917.
[26] W.H. Yuan, Y.Y. Li, P. Dagaut, J.Z. Yang, F. Qi, Investigation on the pyrolysis and oxidation of toluene over a wide range conditions. I. Flow reactor pyrolysis and jet stirred reactor oxidation, Combust. Flame 162 (2015) 3-21.
[27] W.H. Yuan, L. Zhao, S. Gaïl, J.Z. Yang, Y.Y. Li, F. Qi, P. Dagaut, Exploring pyrolysis and oxidation chemistry of *o*-xylene at various pressures with special concerns on PAH formation, Combust. Flame 228 (2021) 351-363.
[28] M. Braun-Unkhoff, P. Frank, T. Just, High temperature reactions of benzyl radicals, Berichte der Bunsengesellschaft für physikalische Chemie 94 (1990) 1417-1425.
[29] A.M. Mebel, A. Landera, R.I. Kaiser, Formation mechanisms of naphthalene and indene: from the interstellar medium to combustion flames, J. Phys. Chem. A 121 (2017) 901-926.
[30] L. Zhao, R.I. Kaiser, B. Xu, U. Ablikim, M. Ahmed, M.V. Zagidullin, V.N. Azyazov, A.H. Howlader, S.F. Wnuk, A.M. Mebel, VUV photoionization study of the formation of the simplest polycyclic aromatic hydrocarbon: Naphthalene ($C_{10}H_8$), J. Phys. Chem. Lett. 9 (2018) 2620-2626.
[31] H.A. Michelsen, M.B. Colket, P.-E. Bengtsson, A. D'anna, P. Desgroux, B.S. Haynes, J.H. Miller, G.J. Nathan, H. Pitsch, H. Wang, A review of terminology used to describe soot formation and evolution under combustion and pyrolytic conditions, ACS Nano 14 (2020) 12470-12490.
[32] N. Hansen, B. Yang, M. Braun-Unkhoff, A. Ramirez, G. Kukkadapu, Molecular-growth pathways in premixed flames of benzene and toluene doped with propyne, Combust. Flame 243 (2022) 112075.
[33] K. Kohse-Höinghaus, Combustion, Chemistry, and Carbon Neutrality, Chem. Rev. 123 (2023) 5139-5219.
[34] G. da Silva, E.E. Moore, J.W. Bozzelli, Decomposition of methylbenzyl radicals in the pyrolysis and oxidation of xylenes, J. Phys. Chem. A 113 (2009) 10264-10278.
[35] P. Hemberger, A.J. Trevitt, T. Gerber, E. Ross, G. da Silva, Isomer-specific product detection of gas-phase xylyl radical

rearrangement and decomposition using VUV synchrotron photoionization, J. Phys. Chem. A 118 (2014) 3593-3604.
[36] K. Pachner, M. Steglich, P. Hemberger, I. Fischer, Photodissociation dynamics of the ortho-and para-xylyl radicals, J. Chem. Phys. 147 (2017) 084303.
[37] W.H. Yuan, Y.Y. Li, P. Dagaut, J.Z. Yang, F. Qi, Investigation on the pyrolysis and oxidation of toluene over a wide range conditions. II. A comprehensive kinetic modeling study, Combust. Flame 162 (2015) 22-40.
[38] W.H. Yuan, Y.Y. Li, G. Pengloan, C. Togbé, P. Dagaut, F. Qi, A comprehensive experimental and kinetic modeling study of ethylbenzene combustion, Combust. Flame 166 (2016) 255-265.
[39] E.R. Ritter, J.W. Bozzelli, THERM: Thermodynamic property estimation for gas phase radicals and molecules, Int. J. Chem. Kinet. 23 (1991) 767-778.
[40] S.W. Benson, Thermochemical kinetics, Wiley1976.
[41] CHEMKIN-PRO 15092, Reaction Design: San Diego.
[42] P. Hemberger, A.J. Trevitt, E. Ross, G. da Silva, Direct observation of para-xylylene as the decomposition product of the meta-xylyl radical using VUV synchrotron radiation, J. Phys. Chem. Lett. 4 (2013) 2546-2550.
[43] T. Stuyver, B. Chen, T. Zeng, P. Geerlings, F. De Proft, R. Hoffmann, Do Diradicals Behave Like Radicals?, Chem. Rev. 119 (2019) 11291-11351.
[44] F. Hirsch, K. Pachner, I. Fischer, K. Issler, J. Petersen, R. Mitric, S. Bakels, A.M. Rijs, Do xylylenes isomerize in pyrolysis?, ChemPhysChem 21 (2020) 1515-1518.
[45] R.G. Miller, M. Stiles, Reaction of benzyne with benzene and naphthalene, J. Am. Chem. Soc. 85 (1963) 1798-1800.
[46] A.S. Savchenkova, I.V. Chechet, S.G. Matveev, M. Frenklach, A.M. Mebel, Formation of phenanthrenyl radicals via the reaction of acenaphthyl with acetylene, Proc. Combust. Inst. 38 (2021) 1441-1448.
[47] V.S. Krasnoukhov, M.V. Zagidullin, I.P. Zavershinskiy, A.M. Mebel, Formation of phenanthrene via recombination of indenyl and cyclopentadienyl radicals: a theoretical study, J. Phys. Chem. A 124 (2020) 9933-9941.
[48] L.B. Tuli, A.M. Mebel, Formation of phenanthrene via H-assisted isomerization of 2-ethynylbiphenyl produced in the reaction of phenyl with phenylacetylene, Int. J. Chem. Kinet. 52 (2020) 875-883.
[49] V. Kislov, A. Sadovnikov, A. Mebel, Formation mechanism of polycyclic aromatic hydrocarbons beyond the second aromatic ring, J. Phys. Chem. A 117 (2013) 4794-4816.
[50] I. Da Costa, R. Eng, A. Gebert, H. Hippler, Direct observation of the rate of H-atom formation in the thermal decomposition of Ortho-, Meta-, and Para-xylene behind shock waves between 1300 and 1800 K, Proc. Combust. Inst. 28 (2000) 1537-1543.